

Uncertainty-Guided Alignment for Unsupervised Domain Adaptation in Regression

Ismail Nejjar

Gaetan Frusque

Florent Forest

Olga Fink

Abstract

Unsupervised Domain Adaptation for Regression (UDAR) aims to adapt a model from a labeled source domain to an unlabeled target domain for regression tasks. Recent successful works in UDAR mostly focus on subspace alignment, involving the alignment of a selected subspace within the entire feature space. This contrasts with the feature alignment methods used for classification, which aim at aligning the entire feature space and have proven effective but are less so in regression settings. Specifically, while classification aims to identify separate clusters across the entire embedding dimension, regression induces less structure in the data representation, necessitating additional guidance for efficient alignment. In this paper, we propose an effective method for UDAR by incorporating guidance from uncertainty. Our approach serves a dual purpose: providing a measure of confidence in predictions and acting as a regularization of the embedding space. Specifically, we leverage the Deep Evidential Learning framework, which outputs both predictions and uncertainties for each input sample. We propose aligning the parameters of higher-order evidential distributions between the source and target domains using traditional alignment methods at the feature or posterior level. Additionally, we propose to augment the feature space representation by mixing source samples with pseudo-labeled target samples based on label similarity. This cross-domain mixing strategy produces more realistic samples than random mixing and introduces higher uncertainty, facilitating further alignment. We demonstrate the effectiveness of our approach on four benchmarks for UDAR, on which we outperform existing methods.

1. Introduction

In the field of machine learning, unsupervised domain adaptation (UDA) has emerged as a prominent research area, particularly for classification tasks [40]. UDA aims to bridge the gap between a labeled source domain and an unlabeled target domain [35]. Despite the success of UDA for

classification, UDA for regression has received relatively less attention. However, many real-world tasks involve continuous target variables. For instance, regression tasks in computer vision, such as depth estimation or age determination based on visual features, involve dealing with continuous target variables. In medical applications, these tasks include forecasting health metrics such as blood pressure levels, while in industrial applications, they encompass condition monitoring and health indicator estimation. Across these applications, data is often subject to domain shifts when collected under varied conditions.

Numerous unsupervised domain adaptation methods have been developed to address the domain shift problem in classification tasks. Common approaches involve aligning the entire feature space [36]. These methods include correlation alignment [32], Maximum Mean Discrepancy [2, 23], and adversarial training [13], aiming to learn domain-invariant representations. However, despite their effectiveness in classification scenarios, these methods have shown poor performance in regression. In contrast to the current state-of-the-art methods in classification, recent advancements in UDAR involve subspace alignment. Notably, methods like Representation Subspace Distance (RSD) [6] and Unsupervised Domain Adaptation Regression by Aligning Inverse Gram Matrices (DARE-GRAM) [28] leverage subspace alignment. The superior performance of subspace alignment over feature alignment methods for regression tasks can be attributed to the nature of classification models, which typically learn distributed representations. These representations distribute discriminative information and patterns associated with each class across various dimensions of the embedding space [17, 20]. This distribution is necessary for the embedding space to form distinct clusters corresponding to different classes, as a class can be considered a semantic superposition of various concepts. In contrast, in regression tasks, regression models tend to learn more focused representations with fewer features strongly correlating with the continuous output. Consequently, regression tasks result in an embedding space with relevant content encoded in fewer dimensions, lacking the richness of information and structure found in the

embeddings learned for classification tasks. This difference between classification and regression underscores the necessity for additional guidance to enhance the effectiveness of feature alignment methods in regression scenarios.

In this paper, we address the aforementioned challenge and enhance the feature representation by introducing uncertainty as a guidance for adaptation. Unlike classification, where confidence estimates are inherently available in model outputs, regression lacks a readily available measure of confidence. The incorporation of uncertainty frameworks serves a dual purpose: it regularizes the feature embedding by predicting both the target output and its associated uncertainty, while also providing a confidence measure in predictions. This measure of confidence becomes instrumental in the adaptation process. To be more specific, a model trained solely on the labeled source domain data is expected to exhibit high uncertainty for unseen target domain data and low uncertainty for source domain data. Aligning the uncertainties of the source and target domains enables the model to dynamically adjust its internal representations. This alignment ensures that the model adapts to the most reliable features for both domains, resulting in a more stable and reliable alignment.

Building upon this idea, we propose Uncertainty-Guided Alignment for unsupervised domain adaptation in regression (UGA). UGA aims to create a rich and structured feature representation by leveraging uncertainty frameworks such as Deep Evidential Regression and Gaussian Processes. We demonstrate that the alignment can be performed not only at the feature level but also at the posterior level. Additionally, we propose augmenting the feature space representation by mixing source samples with pseudo-labeled target samples based on label similarity. This cross-domain mixing strategy produces more realistic samples than random mixing and introduces higher feature discrepancy. Aggregating examples with similar labels while disregarding domain information, contributes to further improving the alignment.

To demonstrate the impact of uncertainty-guided alignment, we evaluate its performance in combination with various feature alignment strategies, including MMD, CORAL, and JDOT, both with and without uncertainty regularization. We showcase the effectiveness of our approach on four domain adaptation benchmarks, revealing a significant improvement in the performance of feature alignment methods when incorporating uncertainty as regularization compared to subspace alignment methods. The main contributions of this work are as follows:

- We propose leveraging uncertainty estimation as guidance for feature alignment for UDAR.
- We demonstrate the flexibility of our proposed framework, as different uncertainty frameworks can be used in combination with different feature alignment methods.

- We show that uncertainty-guided feature alignment is more competitive than subspace alignment methods.
- To enrich the feature space representation, we introduce a mixing strategy, combining source samples with pseudo-labeled target samples based on label similarity.
- We conduct experiments on four UDAR regression benchmarks and demonstrate the superiority of our approach over state-of-the-art methods.

2. Related Work

Unsupervised Domain Adaptation (UDA). In the realm of UDA, two main directions have emerged. The first direction aims to reduce the discrepancy between domains by using optimal transport [3, 8, 10] or matching moments of the distributions through the Maximum Mean Discrepancy (MMD) [4, 23, 24]. The second direction in UDA revolves around learning domain-invariant representations through adversarial learning techniques [5, 13, 29]. In the context of classification, leveraging self-training with confident pseudo-labels has proven to be effective [18, 19, 33, 43]. Furthermore, in the context of UDA, various mixing strategies have been developed to foster domain-invariant representations within the embedding space [37, 38], ultimately enhancing the model’s generalization capabilities. Recent works [41] have approached mixing strategies from a game-theoretical perspective, particularly in constructing the intermediate domain for vision transformers. However, in regression tasks, randomly combining source and target samples may generate unrealistic synthetic sample-label pairs, thereby introducing ambiguity in the target output. This shows the need for alternative mixing strategies for UDAR.

The field of Unsupervised Domain Adaptation for Regression (UDAR) has received relatively less attention compared to classification. Early theoretical works have derived generalization bounds [7, 25, 30]. More recently, Wu et al. [36] proposed a framework for domain adaptation in regression, specifically designed for scenarios where target labels are accessible. This framework encompasses popular approaches, including domain-invariant representation learning, reweighting, and adaptive Gaussian processes. Recent endeavors have focused on tackling the unique challenges within the unsupervised setting for domain adaptation for regression [6, 27, 28]. For instance, RSD [6] addresses the challenge of feature scale changes during domain adaptation by aligning representation subspaces using a geometrical distance measure. Following a similar motivation, DARE-GRAM [28] aligns the angle and scale of the inverse Gram matrices for the source and target features. The authors address ill-conditioned inverse Gram matrices due to the ratio between batch size and the embedding dimension by proposing the use of the pseudo-inverse of the Gram matrix, achieved by selecting a specific subspace. Although feature alignment methods such as adversarial train-

ing and moment matching can be applied in UDAR, their effectiveness is limited in this context. Regression models tend to learn focused representations, causing feature alignment methods to fail as they aim to align the entire feature representation. This motivates the need to structure and enrich the feature representation and provide additional guidance for feature alignment.

Uncertainty-guided domain adaptation Reducing prediction uncertainty on the target domain is a technique that has been explored for domain adaptation. The main intuition is that uncertainty for non-adapted target features is expected to be high, while it is expected to be low for source samples. In the setting of classification, entropy minimization and the related technique of self-training with pseudo-labels, effectively encourage cross-domain feature alignment [15, 42]. In [34], the authors proposed to minimize the uncertainty discrepancy between domains, where uncertainty is measured by the prediction entropy or variance using Monte-Carlo Dropout as an approximate Bayesian variational inference [11]. The approach proposed in [22] aligns the conditional distributions by minimizing the MMD between the mean embeddings of each class. The target distribution class mean embeddings are estimated by a sum of the elements weighted by their posterior probability. In the source-free DA setting, Roy et al. [31] proposed a method based on the information maximization loss but with uncertainty weighting of the samples, using a last-layer Laplace approximation to estimate the uncertainty of the pre-trained model. While our work is closely related to [34] which was applied to classification tasks, its extension to regression tasks is missing. Moreover, the existing studies focused on a narrow scenario, limited to Bayesian neural networks, particularly Monte Carlo Dropout, and adversarial alignment. This paper demonstrates that various uncertainty frameworks, including Gaussian Processes and evidential neural networks, can effectively guide alignment for different feature alignment methods.

3. Preliminaries

Maximum Mean Discrepancy (MMD) [2] is a non-parametric criterion used to quantify the discrepancy between two distributions P and P' by comparing their embeddings in a reproducing kernel Hilbert space (RKHS) \mathcal{H}_k , equipped with a kernel k and an associated feature map $\phi(\mathbf{x})$. Here, $k(\mathbf{x}, \mathbf{x}') = \langle \phi(\mathbf{x}), \phi(\mathbf{x}') \rangle$, where $\langle \mathbf{x}, \mathbf{x}' \rangle$ corresponds to the scalar product between variables \mathbf{x} and \mathbf{x}' . The kernel embedding preserves the distribution properties such as mean, covariance, and higher-order moments if the kernel k is characteristic, such as the radial basis function (RBF) kernel. The squared MMD measures the distance between the expectations of the embeddings of the

distributions P and P' in the RKHS, defined as:

$$\begin{aligned} \text{MMD}^2 &= \|\mathbb{E}_P[\phi(\mathbf{x})] - \mathbb{E}_{P'}[\phi(\mathbf{x}')]\|_{\mathcal{H}_k}^2, \\ &= \mathbb{E}_P[k(\mathbf{x}, \mathbf{x})] - 2\mathbb{E}_{P, P'}[k(\mathbf{x}, \mathbf{x}')] + \mathbb{E}_{P'}[k(\mathbf{x}', \mathbf{x}')] \end{aligned} \quad (1)$$

where $\mathbb{E}[\cdot]$ denotes the expectation with respect to the random variables $\mathbf{x} \sim P$ and $\mathbf{x}' \sim P'$.

Deep Evidential Regression (DER). From a maximum likelihood perspective, the likelihood for the parameters θ given the N observations $\mathbf{X} = \{\mathbf{x}_1, \dots, \mathbf{x}_N\}$ and regression targets $\mathbf{y} = \{y_1, \dots, y_N\}$ is defined as follows:

$$p(\mathbf{y}|\mathbf{X}, \theta) = \prod_{i=1}^N p(y_i|\mathbf{x}_i, \theta) \quad (2)$$

In practice, a common assumption is that the target variable y is drawn from a Gaussian distribution with mean $\mu = f(\mathbf{x}, \theta)$ and variance σ^2 . To explicitly learn both aleatoric and epistemic uncertainties, a common approach, proposed in [1], assumes that the mean and variance of the Gaussian distribution are themselves drawn from higher-order Gaussian and Inverse-Gamma distributions, respectively. This modeling choice allows for the incorporation of prior knowledge about the parameters. Specifically, the Normal Inverse-Gamma (NIG) distribution with parameters $(\gamma, \nu, \alpha, \beta)$, where $\gamma \in \mathbb{R}$, $\nu, \beta > 0$, and $\alpha > 1$, are a higher-order conjugate prior of the Gaussian distribution parameterized by μ, σ^2 . The distributions are defined as:

$$y \sim \mathcal{N}(\mu, \sigma^2), \mu \sim \mathcal{N}(\gamma, \sigma^2/\nu), \sigma^2 \sim \Gamma^{-1}(\alpha, \beta), \quad (3)$$

where $\Gamma(\cdot)$ is the Gamma function. The training minimizes the negative log-likelihood loss given by:

$$\begin{aligned} \mathcal{L}_{\text{NLL}} &= \frac{1}{2} \log\left(\frac{\pi}{\nu}\right) - \alpha \log(2\beta(1 + \nu)) + \log(\psi) \\ &+ \left(\alpha + \frac{1}{2}\right) \log\left(\frac{(y - \gamma)^2 \nu + 2\beta(1 + \nu)}{2\beta(1 + \nu)}\right) \end{aligned} \quad (4)$$

where $\psi = \Gamma(\alpha)/\Gamma(\alpha + 1/2)$. The total evidential loss is defined as the sum of the negative log-likelihood loss and a regularization term:

$$\mathcal{L}_{\text{EVI}} = \mathcal{L}_{\text{NLL}} + \lambda_{\text{EVI}} \mathcal{L}_R, \quad (5)$$

where $\mathcal{L}_R = |y - \gamma|(2\nu + \alpha)$ penalizes evidence of prediction errors, and the coefficient λ_{EVI} balances the trade-off between model fit and increase in uncertainty measure.

4. Method

4.1. Problem setting

Let \mathcal{X} and \mathcal{Y} represent the input space and output space, respectively. In the context of unsupervised domain adaptation, we consider a joint probability distribution P over $\mathcal{X} \times \mathcal{Y}$ within the probability distribution space \mathcal{P} .

With this definition, we have a source domain denoted as S with observation data $\{\mathbf{x}_i^S, y_i^S\}_{i=1}^{N_S}$, which consists

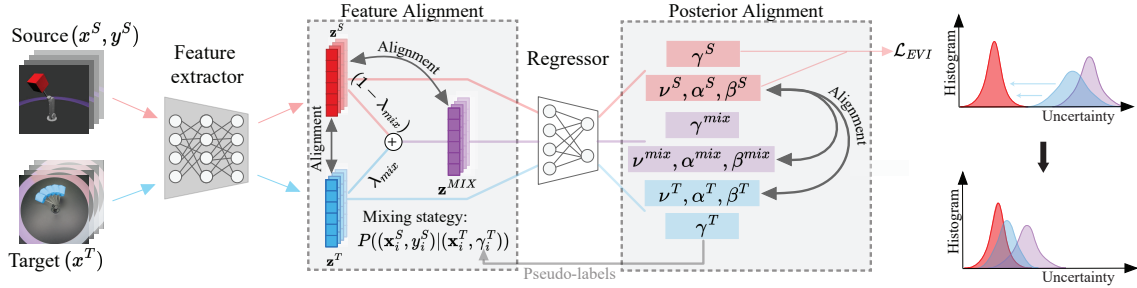


Figure 1. An overview of our proposed Uncertainty-Guided Alignment (UGA) framework for unsupervised domain adaptation in regression. UGA leverages the Deep Evidential Regression (DER) uncertainty framework. We propose aligning augmented feature representations with uncertainty to guide traditional feature alignment. We introduce Posterior alignment, an approximation method aligning evidential distribution parameters. To augment feature representation and improve model generalization, we propose Cross-domain Mixing with pseudo-labels from the target domain, addressing challenges related to unrealistic sample-label pairs that occur with a random mixing strategy.

of labeled samples drawn from the joint probability distribution P_S . Additionally, we have unlabeled observation data $\{\mathbf{x}_i^T\}_{i=1}^{N_T}$ from the target domain T , sampled from the marginal probability distribution P_T . N_S represents the number of labeled samples in the source domain, and N_T is the number of unlabeled samples in the target domain.

Our objective is to predict the continuous-valued outputs y^T of the unlabeled target samples by leveraging the label information from the source domain. We define a model $f(\cdot)$ as the composition of two neural networks, a feature extractor $g(\cdot)$ and regression head $r(\cdot)$. We aim to learn $f: \mathbf{x} \rightarrow y$ parameterized by θ that minimizes the expected error on the target data under the ℓ_2 loss. We assume that the labels cover the same range in both domains.

4.2. Overview of the proposed method

Our proposed method, Uncertainty Guided Adaptation (UGA), addresses the challenge of unsupervised domain adaptation in regression by guiding the alignment of source and target domain distributions using uncertainty. We introduce feature alignment and a variant, termed posterior alignment. Aligning source and target at the feature level ensures alignment of both the predicted target value and uncertainty. Additionally, we propose aligning output uncertainties at the posterior level serving as an *approximation* to the feature alignment method. In both variants, we introduce a novel cross-domain mixing strategy inspired by C-Mixup [39], utilizing pseudo-labels of target samples for selecting source and target samples with similar labels for mixing. Although our framework is versatile and can be combined with different feature alignment methods and uncertainty quantification frameworks, we introduce it using the combination of MMD and DER for brevity and consistency. An overview of our proposed framework is presented in Figure 1.

4.3. Uncertainty quantification

In this paper, we employ uncertainty quantification frameworks to quantify model prediction uncertainty for regression. Bayesian neural networks (BNN) have been the standard approach to quantify uncertainty and consider the weights of the model as distributions. However, performing inference can be computationally expensive as it requires sampling the input multiple times to obtain the output variance. In contrast, evidential deep learning is a standard neural network that treats learning as an evidence-acquisition process, making it computationally more efficient than BNN as it eliminates the need for sampling.

In the following, we introduce two variants of the proposed framework: 1) Uncertainty-Guided Feature Alignment, and 2) Uncertainty-Guided Posterior Alignment.

4.3.1 Uncertainty-Guided Feature Alignment

Uncertainty-Guided Feature Alignment aligns feature embeddings between the source and target domains, similar to [23], with the guidance of uncertainty. Given the sets of feature embeddings for the source and target domains, denoted as $\mathbf{z}_i^S = g(\mathbf{x}_i^S)$ and $\mathbf{z}_i^T = g(\mathbf{x}_i^T)$, respectively, we compute the MMD between their empirical distributions as follows:

$$\text{MMD}_{\text{feature}}^2 = \left\| \frac{1}{N_S} \sum_{i=1}^{N_S} \phi(\mathbf{z}_i^S) - \frac{1}{N_T} \sum_{i=1}^{N_T} \phi(\mathbf{z}_i^T) \right\|_{\mathcal{H}_k}^2. \quad (6)$$

As \mathbf{z}_i encapsulates both the predicted target value and uncertainty, leveraging uncertainty can guide the minimization of feature discrepancy between the source and target domains. The final objective $\mathcal{L}_{\text{feature}}$ can be formulated as :

$$\mathcal{L}_{\text{feature}} = \mathcal{L}_{\text{EVI}} + \lambda \cdot \text{MMD}_{\text{feature}}^2 \quad (7)$$

where λ is a hyperparameter controlling the relative importance of the feature alignment term and \mathcal{L}_{EVI} is the source supervised loss.

4.3.2 Uncertainty-Guided Posterior Alignment

Uncertainty-Guided Posterior Alignment aligns uncertainty distributions between the source and target domains, it aims to align the uncertainty levels directly between the source and target, not necessarily their feature representations. The MMD loss is computed between the higher-order parameters of uncertainty distributions output by the DER models for the source and target samples.

Given the output of the evidential network for the source domain as $\gamma_i^S, \nu_i^S, \alpha_i^S, \beta_i^S = f(\mathbf{x}_i^S)$ and for the target domain as $\gamma_i^T, \nu_i^T, \alpha_i^T, \beta_i^T = f(\mathbf{x}_i^T)$, achieving the alignment of evidence between the source and target domains can be done by minimizing the squared MMD between the higher-order parameters of DER:

$$\begin{aligned} \text{MMD}_{\text{posterior}}^2 = & \left\| \frac{1}{N_S} \sum_{i=1}^{N_S} \phi([\nu_i^S, \alpha_i^S, \beta_i^S]) \right. \\ & \left. - \frac{1}{N_T} \sum_{i=1}^{N_T} \phi([\nu_i^T, \alpha_i^T, \beta_i^T]) \right\|_{\mathcal{H}_k}^2. \end{aligned} \quad (8)$$

This alignment ensures that the uncertainty estimates captured by the evidential network, represented by the parameters ν , α , and β , are consistent and transferable across different domains. The final objective function to be minimized is defined as follows:

$$\mathcal{L}_{\text{posterior}} = \mathcal{L}_{\text{EVI}} + \lambda \cdot \text{MMD}_{\text{posterior}}^2. \quad (9)$$

4.3.3 Mixing strategy for UDAR

We aim to learn domain-transferable and generalized features through a strategic mixing strategy. However, in regression, randomly mixing source and target samples can result in unrealistic synthetic sample-label pairs, introducing ambiguity in the target output. This necessitates alternative mixing strategies for UDAR. Drawing inspiration from C-Mixup [39] and the principle of favoring more similar sample pairs during sampling, we propose its adaptation for cross-domain mixing in unsupervised domain adaptation in regression. We argue that by aggregating examples with similar labels while disregarding domain information, we effectively mitigate the impact of domain-specific variations. Moreover, by taking uncertainty into account, the generated samples are anticipated to exhibit higher levels of feature discrepancy compared to the target samples. This guides the adaptation process, as these samples may not have been encountered by the model before. Since true labels of the target domain are not available during training, we propose using pseudo-labels assigned to target samples as an approximation. This allows the selection of the most similar source samples for mixing.

With \mathbf{x}^S and \mathbf{x}^T representing a source sample and a target sample, respectively, the mixing operation is defined as:

$$\mathbf{x}^{\text{mix}} = \lambda_{\text{mix}} \mathbf{x}^T + (1 - \lambda_{\text{mix}}) \mathbf{x}^S. \quad (10)$$

Here, \mathbf{x}^{mix} denotes the mixed sample, and $\lambda_{\text{mix}} \in [0, 1]$ controls the mixing ratio. We use a symmetric Gaussian kernel to compute the sampling probability for selecting pairs of samples to mix. Given a target domain sample $(\mathbf{x}_i^T, \gamma_i^T)$, where γ_i^T is the model’s predicted target value, our goal is to identify the most similar source domain samples in the current mini-batch for mixing. The sampling probability $P((\mathbf{x}_i^S, y_i^S) | (\mathbf{x}_i^T, \gamma_i^T))$ for a source sample (\mathbf{x}_i^S, y_i^S) to be mixed is determined based on the label similarity:

$$P((\mathbf{x}_i^S, y_i^S) | (\mathbf{x}_i^T, \gamma_i^T)) \propto \exp\left(-\frac{\|y_i^S - \gamma_i^T\|_F^2}{2\sigma_{\text{mix}}^2}\right). \quad (11)$$

The bandwidth parameter σ_{mix} controls the width of the Gaussian kernel. By computing the sampling probabilities based on this kernel, we prioritize selecting source samples whose labels are closer to the target label for the mixing operation. The final optimization problem, including the proposed mixing strategy, is defined as follows:

$$\mathcal{L}_{\text{mix}} = \mathcal{L}_{\text{EVI}} + \lambda \cdot (\text{MMD}^2 + \text{MMD}_{\text{mix}}^2), \quad (12)$$

where MMD^2 represents the alignment loss encouraging similarity between the evidence or feature embeddings of the source and target domains. Similarly, $\text{MMD}_{\text{mix}}^2$ represents the alignment loss, promoting similarity between the evidence or feature embeddings from the source domain and the newly generated cross-domain samples, using either the objective in Eq. 8 or the one in Eq. 6.

5. Experiments

5.1. Experiments Setup

We evaluate our proposed method on four benchmarks: **dSprites** [26] is a synthetic 2D image dataset with five independent latent factors. We treat the dataset three variants as separate domains: Color (**C**), Scream (**S**), and Noise (**N**). Each domain consists of 737,280 images, and we focus on regression domain adaptation tasks for scale and position. **MPI3D** [14] contains 1,036,800 examples of 3D objects from three domains: Toy (**T**), Realistic (**RC**), and Real (**RL**). The dataset enables the study of domain gaps between real and simulated data in a robotics context, focusing on regression tasks involving rotation around vertical and horizontal axes. **Biwi Kinect** [9] dataset consists of over 15,000 real-world images of 20 individuals, including 6 females (**F**) and 14 males (**M**). It captures head rotations with variations in yaw, pitch, and roll angles.

Method	Uncertainty	C → N	C → S	N → C	N → S	S → C	S → N	Avg
Source only model	X	0.94	0.90	0.16	0.65	0.08	0.26	0.498
DANN [13]	X	0.47	0.46	0.16	0.65	0.05	0.10	0.315
RSD [6]	X	0.31	0.31	0.12	0.53	0.07	0.08	0.237
DARE-GRAM [28]	X	0.30	0.20	0.11	0.25	0.05	0.07	0.164
JDOT	X	0.86	0.79	0.19	0.64	0.10	0.23	0.468
UGA-Posterior JDOT (Ours)	DER	0.09	0.13	0.11	0.18	0.05	0.12	0.114
UGA-Feature JDOT (Ours)	DER	0.08	0.11	0.08	0.17	0.05	0.07	0.093
CORAL	X	0.95	0.87	0.13	0.57	0.05	0.12	0.448
UGA-Posterior CORAL (Ours)	DER	0.56	0.40	0.24	0.94	0.04	0.28	0.410
UGA-Feature CORAL (Ours)	DER	0.06	0.24	0.08	0.32	0.02	0.03	0.125
MMD [23]	X	0.70	0.77	0.12	0.50	0.06	0.11	0.377
UGA-Posterior MMD (Ours)	GP	0.05	0.21	0.07	0.55	0.03	0.04	0.158
UGA-Feature MMD (Ours)	GP	0.05	0.19	0.05	0.40	0.03	0.03	0.125
UGA-Posterior MMD (Ours)	DER	0.04	0.10	0.04	0.16	0.03	0.03	0.067
+ C-Mixup	DER	0.03	0.09	0.03	0.14	0.03	0.03	0.058
UGA-Feature MMD (Ours)	DER	0.04	0.10	0.02	0.16	0.02	0.02	0.060
+ C-Mixup	DER	0.03	0.09	0.02	0.13	0.02	0.02	0.052

Table 1. Comparisons with prior studies on the dSprites regression tasks, with results presented as the sum of MAE across the three regression targets. In each experiment, **X** indicates non-use of uncertainty (MSE loss for training), while we mark with uncertainty framework was used respectively Deep Evidential Regression (DER) and Gaussian Processes (GP). For JDOT, CORAL, and MMD, we compare the method with and without uncertainty-guided alignment.

SmallNORB dataset comprises images depicting 50 toys. The images were captured using two cameras, resulting in variations in lighting conditions, elevations, and azimuths. For our experiments, we partitioned the dataset into two domains based on lighting conditions: dark (**D**) and bright (**B**). The objective is to predict the rotation of objects.

Evaluation metrics. In line with previous studies [6, 21], we use Mean Absolute Error (MAE) as the evaluation metric for all regression tasks. Each experiment is repeated three times, and the average results are reported.

5.2. Implementation Details

Training procedure. For the implementation details, we closely followed the experimental setup established in [6]. As the backbone, we used a pre-trained ResNet-18 [16]. The model was modified by disabling the batch normalization layer and adding dropout with a probability of 0.1 after each block. We demonstrate the flexibility of our proposed UGA framework using DER and Gaussian Process (GP). Specifically, we use two GP layers for regression as an approximation of BNN, using the standard implementation of multi-output GPs of GPyTorch. In the case of DER, we use a single linear layer. Unlike the original DER paper, where a small weight is assigned to \mathcal{L}_R , we recognize the importance of this term in our context. This term serves to regularize predicted uncertainty. Given that we train the model to predict uncertainty in the source domain, we strongly penalize the model when the error is high and the uncertainty is low. This approach ensures a well-calibrated uncertainty and provides reliable guidance for adaptation. We used

Adam optimizer with a learning rate of $2e^{-5}$ and weight decay of $1e^{-3}$.

Hyperparameters. In our experiments, we set the hyperparameter λ , in Equations 7 and 9, to increase from 0 to 1, following a similar approach to [12], where $\lambda = \frac{2}{1+\exp(-10p)} - 1$, and p represents the progress of training iterations. λ_{EVI} was set to 1 in all experiments. In C-Mixup, the mixing of source and target features is governed by the parameter λ_{mix} , in Equation 10, which follows a beta distribution $\lambda_{\text{mix}} \sim \text{Beta}(2, 2)$. To control the diversity in mixing, we set the bandwidth parameter σ_{mix} was set to 0.2. For additional details, please refer to the supplementary material. We ensured consistency in the hyperparameter settings across all experiments, unlike RSD and DARE-GRAM, no hyperparameter tuning was performed.

5.3. Results

dSprites: Table 1 presents the results obtained on the dSprites dataset, comparing our proposed methods with existing domain adaptation approaches. Specifically, we consider DANN, RSD, and DARE-GRAM as state-of-the-art methods for UDAR. Additionally, we use three feature alignment methods JDOT, CORAL, and MMD. For each case, we report results obtained without uncertainty guidance and with the proposed frameworks: Feature alignment (UGA-Feature) and Posterior alignment (UGA-Posterior). We also compare results using MMD as a feature alignment method, substituting Deep Evidential Regression (DER) with Gaussian Processes (GP) as uncertainty framework.

In the case of UGA-Feature, aligning the source and tar-

Methods	Uncertainty	RL \rightarrow RC	RL \rightarrow T	RC \rightarrow RL	RC \rightarrow T	T \rightarrow RL	T \rightarrow RC	Avg
Source only model	\times	0.17	0.44	0.19	0.45	0.51	0.50	0.377
Source only model	DER	0.17	0.47	0.14	0.44	0.50	0.48	0.367
DANN [13]	\times	0.09	0.24	0.11	0.41	0.48	0.37	0.283
RSD [6]	\times	0.09	0.19	0.08	0.15	0.36	0.36	0.205
DARE-GRAM [28]	\times	0.08	0.15	0.10	0.14	0.24	0.24	0.160
MMD [23]	\times	0.12	0.35	0.12	0.27	0.40	0.41	0.278
UGA-Posterior MMD (Ours)	DER	0.08	0.45	0.08	0.18	0.41	0.30	0.250
+ C-Mixup	DER	0.07	0.15	0.07	0.12	0.37	0.30	0.180
UGA-Feature MMD (Ours)	DER	0.07	0.13	0.07	0.11	0.34	0.24	0.160
+ C-Mixup	DER	0.08	0.12	0.06	0.12	0.35	0.18	0.152

Table 2. Comparisons with previous works on the MPI3D regression tasks.

get models with any feature alignment method results in a significant performance gain over the standard case without uncertainty guidance. Specifically, for JDOT, CORAL, and MMD, the average MAE without using uncertainty is 0.468, 0.448, and 0.377, respectively. With the inclusion of uncertainty, these values are notably reduced to 0.09, 0.125, and 0.06. Moreover, these methods outperform previous state-of-the-art methods such as RSD and DARE-GRAM, achieving an MAE of 0.237 and 0.164.

In the case of UGA-Posterior, a notable improvement is observed for JDOT and MMD with the inclusion of uncertainty. In comparison to the SOTA models RSD and DARE-GRAM, the proposed framework results in a relative improvement of at least 34% and 4%, respectively. For CORAL, the improvement with the addition of an uncertainty framework is relatively small, with the MAE reducing from 0.448 to 0.410. This might be attributed to the simplicity of the CORAL method, which does not effectively align the higher-order evidence. We evaluate the impact of C-Mixup in promoting better alignment and improving generalization. UGA-Posterior+C-Mixup achieves an average MAE of 0.058, with a relative improvement of 13% over UGA-Posterior alone. Similarly, UGA-Feature+C-Mixup achieves an average MAE of 0.052, with a relative improvement of 13% over UGA-Feature alone.

Guiding the alignment with GP and DER results in a significant improvement in the average MAE across all tasks compared to alignment without uncertainty. Since the best combination is achieved using MMD and DER, we only focus on this pairing for the remaining results.

MPI3D: Table 2 presents the result obtained on the MPI3D dataset. Our proposed methods exhibit superior performance in five out of six tasks and achieve the best average performance. Across the six tasks, posterior alignment achieves an average MAE of 0.250, while feature alignment achieves an average MAE of 0.160. However, in the T \rightarrow RL task, DARE-GRAM outperforms our proposed methods, with an MAE of 0.24, compared to UGA-Feature’s MAE of 0.34. In the appendix, we present the histogram of predicted values and observe that for the T \rightarrow RL task, the model strug-

gles to predict values near the boundary (0 or 1), unlike the behavior in the RC \rightarrow T task. Furthermore, the incorporation of C-Mixup into posterior alignment yields notable improvements for the RC \rightarrow T and RL \rightarrow T tasks. The addition of C-Mixup reduces the MAE from 0.45 to 0.15 for the RC \rightarrow T task and from 0.18 to 0.12 for the RL \rightarrow T task. We also compared the source-only model with and without uncertainty, and the average MAE on the target domain remains similar. This indicates that the performance improvement does not stem from the uncertainty regularization itself but from the guidance it provides.

Method	Biwi Kinect			SmallNorb		
	M \rightarrow F	F \rightarrow M	Avg	B \rightarrow D	D \rightarrow B	Avg
ResNet-18	0.29	0.38	0.335	0.22	0.14	0.180
DANN	0.30	0.37	0.335	0.17	0.11	0.140
RSD	0.26	0.30	0.280	0.17	0.10	0.135
DARE-GRAM	0.23	0.29	0.260	0.18	0.11	0.145
MMD	0.28	0.37	0.325	0.18	0.10	0.140
UGA-Posterior	0.18	0.25	0.215	0.06	0.04	0.050
+ C-Mixup	0.21	0.27	0.240	0.07	0.06	0.065
UGA-Feature	0.30	0.32	0.310	0.05	0.03	0.040
+ C-Mixup	0.33	0.34	0.335	0.05	0.03	0.040

Table 3. MAE error on Biwi Kinect and SmallNorb.

Biwi Kinect and SmallNorb: Table 3 presents the results obtained on the Biwi Kinect and SmallNorb datasets. On both datasets, the addition of uncertainty prediction using DER and MMD for feature alignment improves upon the setup of using MMD without uncertainty. On Biwi Kinect, Posterior alignment achieves the lowest MAE of 0.215, showcasing its effectiveness in addressing the domain adaptation challenge for this task. In contrast, Feature alignment performs relatively poorly on this particular dataset. Unexpectedly, incorporating C-Mixup does not yield improved results in this real-world scenario. This may be attributed to the varying camera orientations, the proposed mixing strategy cannot compensate for this and creates unrealistic sample-labels pairs. On SmallNorb, UGA-Posterior and UGA-Feature outperform RSD with a relative improvement of 60% and 68% in average prediction over both tasks.

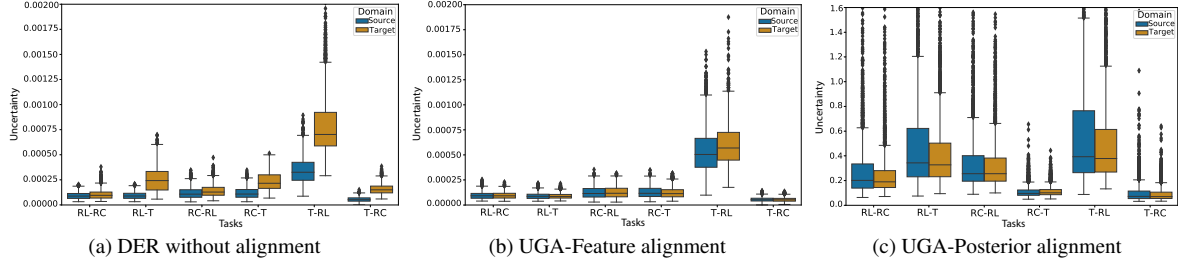


Figure 2. Uncertainty between the source and target domain comparison across different tasks.

5.4. Ablation study

Comparison between Mixup and C-Mixup. Table 4 provides a comparison of our proposed methods on the MPI3D dataset, Posterior alignment, and Feature alignment when using standard Mixup and C-Mixup. We observe that C-Mixup consistently outperforms Mixup in terms of MAE across all tasks. For example, in the RL→T task, C-Mixup reduces the MAE from 0.23 to 0.15 for Posterior alignment and from 0.13 to 0.12 for Feature alignment.

Uncertainty minimization. As a baseline method, we trained the network to minimize the uncertainty predicted for each observation in the target domain, similar to entropy minimization. However, our experimental results, presented in Table 4, reveal that this strategy does not effectively contribute to the alignment between the source and target domains. Despite the attempts to reduce the uncertainty, the MAE values obtained using this approach are consistently higher than our proposed methods. This is because the similarity of the two ratios (i.e., $\frac{\beta^T}{\nu^T(\alpha^T-1)}$ and (i.e., $\frac{\beta^S}{\nu^S(\alpha^S-1)}$)) does not imply β^S is similar to β^T and α^S is similar to α^T .

C-Mixup In Figure 3, we present the domain loss associated with the discrepancy between the source and target domains and between the source and mixed domains. We can observe that the discrepancy between the mixed samples and the source samples is higher at the beginning of the training process than the discrepancy between the target and source samples.

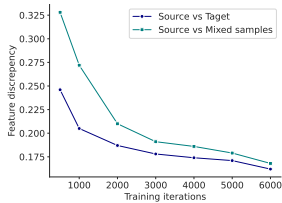


Figure 3. Discrepancy loss across the training process.

Method	Avg
UGA-Post. + Mixup	0.207
UGA-Post. + C-Mixup	0.180
UGA-Feat.+ Mixup	0.162
UGA-Feat. + C-Mixup	0.152
Uncertainty min.	0.358
UGA-Post.	0.250

Table 4. Comparing Mixup and C-Mixup on MPI3D.

5.5. Discussion

Our proposed framework demonstrate promising results across various benchmarks. While Feature alignment excels in terms of MAE on most benchmarks, Posterior alignment proves to be a viable alternative. Moreover, the integration

of C-Mixup leads to notable improvements, particularly in the RC→T and RL→T tasks for Posterior alignment, and in the T→RC task for feature alignment on MPI3D. Figure 2 presents a box plot displaying uncertainties for both source and target domains on the MPI3D dataset without alignment and with both alignment strategies. The figure illustrates a clear correlation between disparities in uncertainties within the source and target domains and the resulting error observed in the target domain. Furthermore, the uncertainty in the target domain is reduced after alignment, but posterior alignment results in much higher uncertainty levels in general.

When comparing Posterior and Feature alignment, their distinctions lie in their objectives. Posterior alignment specifically addresses uncertainty alignment at the output level, but it can lead to high uncertainty in both domains. On the other hand, feature-level alignment aims to prevent an increase in the uncertainty of the source during alignment. Minimizing cross-domain uncertainty discrepancies encourages the feature extractor to generate target features that align better with the source. The uncertainty obtained with UGA-Feature is well-aligned between the source and target domains, with a noticeable deviation observed in the T→RL task. For this specific task, our approach performs worse than DARE-GRAM.

6. Conclusion

In this paper, we propose Uncertainty-Guided Alignment (UGA) for unsupervised domain adaptation in regression tasks. In contrast to previous methods in UDAR that mainly focus on subspace alignment, we leverage uncertainty-guided feature alignment methods, highlighting their limitations in regression settings and the need for additional guidance. Our framework is general, combining any feature alignment methods with uncertainty estimators. Additionally, we proposed a mixing strategy for model generalization with richer feature representation by combining source and pseudo-labeled target samples based on label similarity. Extensive experiments on four benchmarks demonstrate the superiority of UGA over previous methods, highlighting its effectiveness in improving adaptation performance and its potential for real-world regression applications.

References

- [1] Alexander Amini, Wilko Schwarting, Ava Soleimany, and Daniela Rus. Deep evidential regression. *Advances in Neural Information Processing Systems*, 33:14927–14937, 2020. [3](#)
- [2] Karsten M Borgwardt, Arthur Gretton, Malte J Rasch, Hans-Peter Kriegel, Bernhard Schölkopf, and Alex J Smola. Integrating structured biological data by kernel maximum mean discrepancy. *Bioinformatics*, 22(14):e49–e57, 2006. [1](#), [3](#)
- [3] Wanxing Chang, Ye Shi, Hoang Tuan, and Jingya Wang. Unified optimal transport framework for universal domain adaptation. *Advances in Neural Information Processing Systems*, 35:29512–29524, 2022. [2](#)
- [4] Chao Chen, Zhihang Fu, Zhihong Chen, Sheng Jin, Zhaowei Cheng, Xinyu Jin, and Xian-Sheng Hua. Homm: Higher-order moment matching for unsupervised domain adaptation. In *Proceedings of the AAAI conference on artificial intelligence*, pages 3422–3429, 2020. [2](#)
- [5] Lin Chen, Huaian Chen, Zhixiang Wei, Xin Jin, Xiao Tan, Yi Jin, and Enhong Chen. Reusing the task-specific classifier as a discriminator: Discriminator-free adversarial domain adaptation. In *Proceedings of the IEEE/CVF Conference on Computer Vision and Pattern Recognition*, pages 7181–7190, 2022. [2](#)
- [6] Xinyang Chen, Sinan Wang, Jianmin Wang, and Mingsheng Long. Representation subspace distance for domain adaptation regression. In *International Conference on Machine Learning*, pages 1749–1759. PMLR, 2021. [1](#), [2](#), [6](#), [7](#)
- [7] Corinna Cortes and Mehryar Mohri. Domain Adaptation in Regression. In *Algorithmic Learning Theory*, pages 308–323, Berlin, Heidelberg, 2011. Springer. [2](#)
- [8] Nicolas Courty, Remi Flamary, Devis Tuia, and Alain Rakotomamonjy. Optimal Transport for Domain Adaptation. *IEEE Transactions on Pattern Analysis and Machine Intelligence*, 39(9):1853–1865, 2017. [2](#)
- [9] Gabriele Fanelli, Matthias Dantone, Juergen Gall, Andrea Fossati, and Luc Van Gool. Random forests for real time 3d face analysis. *Int. J. Comput. Vision*, 101(3):437–458, 2013. [5](#)
- [10] Kilian Fatras, Thibault Séjourné, Rémi Flamary, and Nicolas Courty. Unbalanced minibatch optimal transport; applications to domain adaptation. In *International Conference on Machine Learning*, pages 3186–3197. PMLR, 2021. [2](#)
- [11] Yarín Gal and Zoubin Ghahramani. Dropout as a bayesian approximation: Representing model uncertainty in deep learning. In *international conference on machine learning*, pages 1050–1059. PMLR, 2016. [3](#)
- [12] Yaroslav Ganin and Victor Lempitsky. Unsupervised domain adaptation by backpropagation. In *International conference on machine learning*, pages 1180–1189. PMLR, 2015. [6](#)
- [13] Yaroslav Ganin, Evgeniya Ustinova, Hana Ajakan, Pascal Germain, Hugo Larochelle, François Laviolette, Mario Marchand, and Victor Lempitsky. Domain-adversarial training of neural networks. *The journal of machine learning research*, 17(1):2096–2030, 2016. [1](#), [2](#), [6](#), [7](#)
- [14] Muhammad Waleed Gondal, Manuel Wuthrich, Djordje Miladinovic, Francesco Locatello, Martin Breidt, Valentin Volchkov, Joel Akpo, Olivier Bachem, Bernhard Schölkopf, and Stefan Bauer. On the transfer of inductive bias from simulation to the real world: a new disentanglement dataset. In *Advances in Neural Information Processing Systems*. Curran Associates, Inc., 2019. [5](#)
- [15] Ligong Han, Yang Zou, Ruijiang Gao, Lezi Wang, and Dimitris Metaxas. Unsupervised domain adaptation via calibrating uncertainties. In *CVPR Workshops*, 2019. [3](#)
- [16] Kaiming He, Xiangyu Zhang, Shaoqing Ren, and Jian Sun. Deep residual learning for image recognition, 2015. [6](#)
- [17] Geoffrey E Hinton. Distributed representations. 1984. [1](#)
- [18] Lukas Hoyer, Dengxin Dai, Haoran Wang, and Luc Van Gool. Mic: Masked image consistency for context-enhanced domain adaptation. In *Proceedings of the IEEE/CVF Conference on Computer Vision and Pattern Recognition*, pages 11721–11732, 2023. [2](#)
- [19] Nazmul Karim, Niluthpol Chowdhury Mithun, Abhinav Rajvanshi, Han-pang Chiu, Supun Samarasekera, and Nazanin Rahnavard. C-sfda: A curriculum learning aided self-training framework for efficient source free domain adaptation. In *Proceedings of the IEEE/CVF Conference on Computer Vision and Pattern Recognition*, pages 24120–24131, 2023. [2](#)
- [20] Yann LeCun, Yoshua Bengio, and Geoffrey Hinton. Deep learning. *nature*, 521(7553):436–444, 2015. [1](#)
- [21] Wanhua Li, Xiaoke Huang, Jiwen Lu, Jianjiang Feng, and Jie Zhou. Learning probabilistic ordinal embeddings for uncertainty-aware regression. In *Proceedings of the IEEE/CVF Conference on Computer Vision and Pattern Recognition*, pages 13896–13905, 2021. [6](#)
- [22] Jian Liang, Ran He, Zhenan Sun, and Tieniu Tan. Exploring uncertainty in pseudo-label guided unsupervised domain adaptation. *Pattern Recognition*, 96:106996, 2019. [3](#)
- [23] Mingsheng Long, Yue Cao, Jianmin Wang, and Michael Jordan. Learning transferable features with deep adaptation networks. In *International conference on machine learning*, pages 97–105. PMLR, 2015. [1](#), [2](#), [4](#), [6](#), [7](#)
- [24] You-Wei Luo and Chuan-Xian Ren. Conditional bures metric for domain adaptation. In *Proceedings of the IEEE/CVF Conference on Computer Vision and Pattern Recognition (CVPR)*, pages 13989–13998, 2021. [2](#)
- [25] Yishay Mansour, Mehryar Mohri, and Afshin Rostamizadeh. Domain Adaptation: Learning Bounds and Algorithms, 2009. arXiv:0902.3430 [cs]. [2](#)
- [26] Loic Matthey, Irina Higgins, Demis Hassabis, and Alexander Lerchner. dsprites: Disentanglement testing sprites dataset. <https://github.com/deepmind/dsprites-dataset/>, 2017. [5](#)
- [27] Ismail Nejjar, Fabian Geissmann, Mengjie Zhao, Cees Taal, and Olga Fink. Domain adaptation via alignment of operation profile for remaining useful lifetime prediction. *arXiv preprint arXiv:2302.01704*, 2023. [2](#)
- [28] Ismail Nejjar, Qin Wang, and Olga Fink. Dare-gram: Unsupervised domain adaptation regression by aligning inverse gram matrices. In *Proceedings of the IEEE/CVF Conference on Computer Vision and Pattern Recognition (CVPR)*, pages 11744–11754, 2023. [1](#), [2](#), [6](#), [7](#)
- [29] Harsh Rangwani, Sumukh K Aithal, Mayank Mishra, Arihant Jain, and Venkatesh Babu Radhakrishnan. A closer

- look at smoothness in domain adversarial training. In *International Conference on Machine Learning*, pages 18378–18399. PMLR, 2022. 2
- [30] Ievgen Redko, Emilie Morvant, Amaury Habrard, Marc Sebban, and Younès Bennani. A survey on domain adaptation theory: learning bounds and theoretical guarantees, 2022. arXiv:2004.11829 [cs, stat]. 2
- [31] Subhankar Roy, Martin Trapp, Andrea Pilzer, Juho Kannala, Nicu Sebe, Elisa Ricci, and Arno Solin. Uncertainty-guided source-free domain adaptation. In *European Conference on Computer Vision*, pages 537–555. Springer, 2022. 3
- [32] Baochen Sun and Kate Saenko. Deep coral: Correlation alignment for deep domain adaptation. In *European conference on computer vision*, pages 443–450. Springer, 2016. 1
- [33] Tao Sun, Cheng Lu, Tianshuo Zhang, and Haibin Ling. Safe self-refinement for transformer-based domain adaptation. In *Proceedings of the IEEE/CVF conference on computer vision and pattern recognition*, pages 7191–7200, 2022. 2
- [34] Jun Wen, Nenggan Zheng, Junsong Yuan, Zhefeng Gong, and Changyou Chen. Bayesian uncertainty matching for unsupervised domain adaptation. *arXiv preprint arXiv:1906.09693*, 2019. 3
- [35] Garrett Wilson and Diane J. Cook. A survey of unsupervised deep domain adaptation. *ACM Trans. Intell. Syst. Technol.*, 11(5), 2020. 1
- [36] Jun Wu, Jingrui He, Sheng Wang, Kaiyu Guan, and Elizabeth Ainsworth. Distribution-informed neural networks for domain adaptation regression. In *Advances in Neural Information Processing Systems*, 2022. 1, 2
- [37] Yuan Wu, Diana Inkpen, and Ahmed El-Roby. Dual mixup regularized learning for adversarial domain adaptation. *CoRR*, abs/2007.03141, 2020. 2
- [38] Minghao Xu, Jian Zhang, Bingbing Ni, Teng Li, Chengjie Wang, Qi Tian, and Wenjun Zhang. Adversarial domain adaptation with domain mixup, 2019. 2
- [39] Huaxiu Yao, Yiping Wang, Linjun Zhang, James Y Zou, and Chelsea Finn. C-mixup: Improving generalization in regression. *Advances in Neural Information Processing Systems*, 35:3361–3376, 2022. 4, 5
- [40] Yuchen Zhang, Tianle Liu, Mingsheng Long, and Michael Jordan. Bridging theory and algorithm for domain adaptation. In *International conference on machine learning*, pages 7404–7413. PMLR, 2019. 1
- [41] Jinjing Zhu, Haotian Bai, and Lin Wang. Patch-mix transformer for unsupervised domain adaptation: A game perspective. In *Proceedings of the IEEE/CVF Conference on Computer Vision and Pattern Recognition (CVPR)*, pages 3561–3571, 2023. 2
- [42] Yang Zou, Zhiding Yu, BVK Kumar, and Jinsong Wang. Unsupervised domain adaptation for semantic segmentation via class-balanced self-training. In *Proceedings of the European conference on computer vision (ECCV)*, pages 289–305, 2018. 3
- [43] Yang Zou, Zhiding Yu, B. V. K. Vijaya Kumar, and Jinsong Wang. Domain Adaptation for Semantic Segmentation via Class-Balanced Self-Training, 2018. arXiv:1810.07911 [cs]. 2

Supplementary Material for Uncertainty-Guided Alignment for Unsupervised Domain Adaptation in Regression

Anonymous CVPR submission

Paper ID 14884

In this supplementary material for the proposed framework for Uncertainty-Guided Alignment for Unsupervised Domain Adaptation in Regression, we provide additional discussions on the transferability, implementation, and discuss limitations of our method.

In Section 2, we first present insights on the label mismatch that occurs in UDAR. In Section 2, we present an additional analysis of the different mixing strategies. Furthermore, an ablation study is presented in Section 3 to compare an alternative strategy to uncertainty alignment. In section 4, we conduct an experiment on the impact of the batch normalization layers for regression tasks. Additional dataset information and implementation details are also presented in Section 7, 5 and 6. In Section 8, we discuss the limitations of our method. Our code for the main paper is also attached.

1. Label Mismatch

The proposed methodology effectively mitigated the label mismatch by leveraging uncertainty to guide the alignment. As seen in Figure 1, a model without adaptation, typically predicts values around 0.5, which is the expected value of the target label distribution. We propose uncertainty-guided alignment, wherein we align the uncertainty between the source and target domains. This indirectly forces the prediction distributions to be similar, thereby mitigating the impact of label mismatch.

2. Mixing strategies

2.1. Results on Mixup vs C-Mixup

In this supplementary, we provide a comprehensive table comparing Mixup and C-Mixup.

2.2. Manifold C-mixup vs Input C-mixup

We compare the effectiveness of two different data augmentation techniques, namely Manifold C-mixup and Input C-mixup, for domain adaptation tasks. Specifically, we eval-

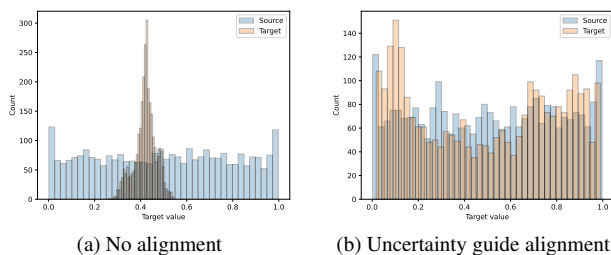


Figure 1. Distribution predictions on source and target domain for model with and without adaptation.

Method	RL → RC	RL → T	RC → RL	RC → T	T → RL	T → RC	Avg
UGA-Post. + Mixup	0.07	0.23	0.09	0.16	0.37	0.32	0.207
UGA-Post. + C-Mixup	0.07	0.15	0.07	0.12	0.37	0.30	0.180
UGA-Feat. + Mixup	0.08	0.13	0.07	0.13	0.36	0.20	0.162
UGA-Feat. + C-Mixup	0.08	0.12	0.06	0.12	0.35	0.18	0.152
Uncertainty min.	0.17	0.48	0.12	0.43	0.48	0.47	0.358
UGA-Post.	0.08	0.45	0.08	0.18	0.41	0.30	0.250

Table 1. Ablation study on MPI3D comparing Mixup vs C-Mixup, and our method vs an uncertainty minimization baseline. All results are shown as the sum of MAE across the regression targets.

uate their performance in improving the generalization capabilities of models across different domains. In the paper, we reported the results using Manifold C-mixup, since they have shown the best performance.

Methods	RL → RC	RL → T	RC → RL	RC → T	T → RL	T → RC	Avg
C-Mixup Manifold	0.07	0.15	0.07	0.12	0.37	0.30	0.180
C-Mixup Input	0.07	0.13	0.08	0.19	0.37	0.31	0.192

Table 2. Performance comparison of Manifold C-Mixup and Input C-Mixup using UGA-Posterior on the MPI3D regression tasks.

We compare the performance of Manifold C-mixup and Input C-mixup on domain adaptation tasks using the MPI3D regression dataset. Table 2 presents the results for the UGA-Posterior approach, and Table 3 shows the results for the UGA-Feature approach. From the tables, it can be observed that Manifold C-mixup consistently achieves

Methods	RL → RC	RL → T	RC → RL	RC → T	T → RL	T → RC	Avg
C-Mixup Manifold	0.08	0.12	0.06	0.12	0.35	0.18	0.152
C-Mixup Input	0.07	0.12	0.07	0.10	0.38	0.24	0.163

Table 3. Performance comparison of Manifold C-Mixup and Input C-Mixup using UGA-Feature on the MPI3D regression tasks.

lower MAE values compared to Input C-mixup. This indicates that Manifold C-mixup is more effective in improving the generalization performance of the models across different domain adaptation tasks. It is important to note that the hyperparameters for Manifold C-mixup were selected based on the experimental setup described in the paper.

3. Uncertainty minimization

In this ablation study, we investigated two distinct approaches for domain adaptation, namely uncertainty minimization and posterior alignment, with a particular focus on evaluating their effectiveness on the test set of the T→RC task for both the source and target domains. The estimated epistemic uncertainty from the Deep evidential network can be computed as $\frac{\beta}{\nu(\alpha-1)}$.

In the uncertainty minimization approach based on the output parameter, we employed a Deep evidential network to estimate the uncertainty of model predictions and incorporated a term to minimize the epistemic uncertainty for both the source and target domains. Surprisingly, we observed remarkably low computed epistemic uncertainties of 0.0004 for both domains. However, upon closer examination of the box plots in figure 2, notable differences emerged in the predicted parameters, particularly alpha and nu, between the two domains. The source domain exhibited tighter and smaller parameter values compared to the target domain. Despite the model’s overconfident predictions, this approach resulted in a relatively high MAE of 0.47 compared to 0.30 MAE obtained with Posterior alignment.

Conversely, in our posterior alignment approach, we focused on aligning the uncertainties of the model’s output. We observed a high epistemic uncertainty of 0.20 for the target domain and 0.24 for the source domain. Interestingly, this less confident approach yielded improved performance on the test dataset, achieving a lower MAE of 0.30 compared to an MAE of 0.47 obtained with uncertainty minimization. Additionally, it is worth noting that in figure 3, the evidential parameters exhibited similar values for both the source and target domains.

Approach	MAE	Estimated Uncertainty
Uncertainty Minimization	0.47	0.0004 (target), 0.0004 (source),
Posterior Alignment	0.30	0.20 (target), 0.24 (source)

Table 4. MAE and estimated uncertainties for uncertainty minimization and posterior alignment approaches.

The findings presented in Table 4 strongly emphasize the significance of incorporating uncertainty measures and examining the predicted parameter values when evaluating the model’s performance. The observed differences in parameter distributions between the source and target domains imply underlying disparities in data distributions and the model’s ability to capture them accurately. Moreover, despite larger errors, the model’s overconfidence in the target domain highlights a potential limitation in its calibration.

Overall, our ablation study highlights the difference between uncertainty minimization and posterior alignment in the context of domain adaptation. While uncertainty minimization resulted in overconfidence and higher errors, posterior alignment introduced higher uncertainties, but ultimately resulted in improved performance.

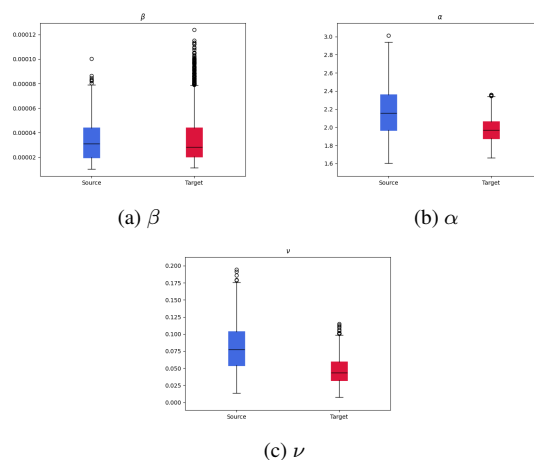


Figure 2. Analysis of deep Evidential Network Parameters in Uncertainty Minimization: T→RC Task

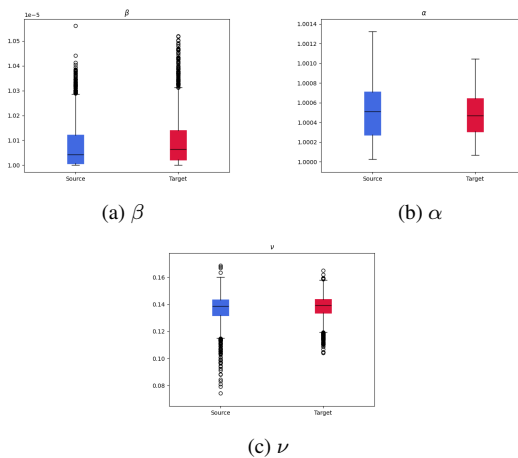


Figure 3. Analysis of deep Evidential Network Parameters in posterior alignment: T→RC Task

098	4. Ablation Study and Impact of Batch Normalization	
099		
100	Ablation Study on ResNet-18 Backbone. Table 5 presents	
101	the results of an ablation study conducted on the MPI3D	
102	regression tasks using a ResNet-18 backbone. The study	
103	compares different combinations of methods involving the	
104	presence or absence of batch normalization (BN) and the	
105	utilization of the evidential loss function (EVI) in compar-	
106	ison to the mean square error loss (MSE).	
107	Among the setups considered in the ablation study, the	
108	”MSE & BN” method represents the standard approach and	
109	achieved an average MAE of 0.377 across all six domain	
110	adaptation tasks. This setup serves as the baseline for com-	
111	parison with other setups and provides a reference point for	
112	evaluating their performance.	
113	Interestingly, ”EVI & BN” and ”EVI & no BN” achieved	
114	slightly better results, suggesting that the evidential loss	
115	function alone can contribute to effective regularization of	
116	the feature embeddings compared to the standard MSE loss,	
117	even without the use of batch normalization.	
118	This ablation study highlights the impact of different	
119	setup combinations on the performance of the ResNet-18	
120	backbone in the MPI3D regression tasks. The inclusion of	
121	the evidential loss function, either with or without batch	
122	normalization, showed promise in improving the model’s	
123	performance across various domain adaptation scenarios.	
124	Impact of Batch-Normalization on UGA. In our experi-	
125	ments, we also investigated the impact of Batch Normaliza-	
126	tion (BN) on the performance of our UGA-Posterior and	
127	UGA-Feature methods. Table 6 presents the results ob-	
128	tained with and without Batch Normalization for both meth-	
129	ods on the MPI3D regression tasks using a ResNet-18.	
130	Interestingly, our experiments revealed that disabling	
131	Batch Normalization (BN) resulted in improved perfor-	
132	mance for both UGA-Posterior and UGA-Feature methods.	
133	Given these findings, our paper specifically used the model	
134	with disabled batch normalization for all experiments.	
135	5. Time Complexity Analysis	
136	This section analyzes the time complexities of different do-	
137	main adaptation methods for regression. We measure the	
138	average time required for one iteration of training and com-	
139	pare the computational efficiency of each method. To con-	
140	duct our experiments, we used an NVIDIA 3090 GPU and	
141	an Intel Xeon CPU.	
142	The average time required for one iteration, encompass-	
143	ing both forward and backward passes, was measured for	
144	each method, as shown in Table 7. UGA with Poste-	
145	rior Alignment achieved the lowest time complexity, with	
146	an average of 0.13 seconds per iteration. In comparison,	
147	both UGA with Manifold Mixing and RSD exhibited simi-	
148	lar time complexities, averaging 0.22 seconds per iteration.	
	However, DAREGRAM displayed a slightly higher time	149
	complexity with an average of 0.33 seconds per iteration.	150
	The higher time complexities of RSD and DAREGRAM	151
	can be attributed to their reliance on singular value decom-	152
	position (SVD) for their operations. SVD involves compu-	153
	tationally intensive calculations, leading to increased time	154
	requirements.	155
	6. Implementation details	156
	In this section, we present the implementation details of our	157
	approach.	158
	Label Scaling. To tackle the issue of diverse scales in re-	159
	gression values, we normalize the source and target labels	160
	to a common range of $[0, 1]$. This normalization process	161
	ensures a consistent scale across the tasks and facilitates ef-	162
	fective comparison and evaluation.	163
	Learning Rate Schedule. We adopt a learning rate sched-	164
	uler inspired by the works of [? ?]. The learning	165
	rate, denoted as η , is determined by the formulation $\eta =$	166
	$\eta_0 \cdot (1 + 0.0001p)^{-0.75}$, where p represents the number of	167
	iterations ranging from 0 to the maximum number of itera-	168
	tions.	169
	Iterations. The number of iterations for each experiment	170
	is determined according to [?]. Specifically, we set it to	171
	20,000 iterations for the dSprites dataset, 10,000 for the	172
	MPI3D dataset (2,000 for T→RL task, and we use a learn-	173
	ing rate ten times high for the regressor), and 10,000 for the	174
	Biwi Kinect dataset. These choices align with the experi-	175
	mental setup of RSD [?] and DAREGRAM[?].	176
	Preprocessing and Batching. Prior to training, we pre-	177
	process the input images by resizing them to dimensions of	178
	224×224 and use a batch of size $b = 36$.	179
	7. Benchmark regression task	180
	We evaluated our proposed method in the main paper on	181
	four domain adaptations for regression. Three are bench-	182
	mark datasets used in previous works: dSprites, MPI3D,	183
	Biwi Kinect, and for the fourth one we used SmallNorb.	184
	dSprites: The dSprites dataset is a widely used benchmark	185
	for domain adaptation in regression tasks. It consists of im-	186
	ages that depict 2D shapes rendered on a gray background.	187
	Each shape is rendered with various variations in factors	188
	such as scale, orientation, position, and shape type. In	189
	our evaluation, we considered three distinct domains of the	190
	dSprites dataset, namely Color (C), Scream (S), and Noise	191
	(N), as illustrated in Figure 4.	192
	Figure 4 showcases example images from each domain,	193
	highlighting the differences between them. The Noise do-	194
	main represents images with added noise, which introduces	195
	additional variation and challenges in regression tasks. The	196
	Color domain depicts shapes with different color variations,	197
	while the Scream domain presents shapes with exaggerated	198

Methods	RL \rightarrow RC	RL \rightarrow T	RC \rightarrow RL	RC \rightarrow T	T \rightarrow RL	T \rightarrow RC	Avg
MSE & BN	0.17	0.44	0.19	0.45	0.51	0.50	0.377
EVI & BN	0.11	0.46	0.15	0.42	0.48	0.44	0.343
EVI & no BN	0.17	0.47	0.14	0.44	0.50	0.48	0.367

Table 5. Resnet-18 backbone with and without Batch-norm and with and without Evidential loss on the MPI3D regression tasks.

Methods	RL \rightarrow RC	RL \rightarrow T	RC \rightarrow RL	RC \rightarrow T	T \rightarrow RL	T \rightarrow RC	Avg
UGA-Posterior & BN	0.07	0.37	0.14	0.23	0.47	0.38	0.277
UGA-Posterior & no BN	0.08	0.45	0.08	0.18	0.41	0.30	0.250
UGA-Feature & BN	0.07	0.18	0.12	0.15	0.43	0.41	0.237
UGA-Feature & no BN	0.07	0.13	0.07	0.11	0.34	0.24	0.160

Table 6. UGA approach with and without Batch-norm on the MPI3D regression tasks.

Methods	Time per Iteration (seconds)
UGA-Posterior	0.13
UGA-Manifold Mixing	0.22
RSD	0.22
DAREGRAM	0.33

Table 7. Time per iteration for domain adaptation methods.

Factor	Values	Task
Scale	6 values in $[0.5, 1]$	Regression
Orientation	40 values in $[0, 2\pi]$	Regression
Position X	32 values in $[0, 1]$	Regression
Position Y	32 values in $[0, 1]$	Regression
Shape Y	3 values	Classification

Table 8. Variations factor values on dSprites dataset

199 expressions or deformations.

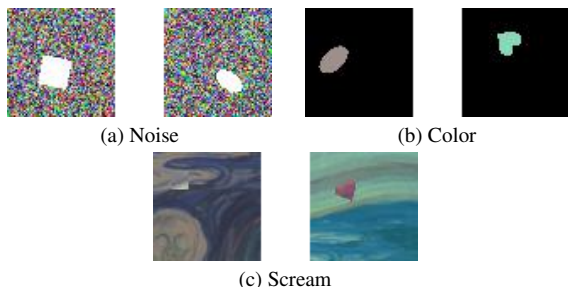


Figure 4. Sample example of different domains in dSprites.

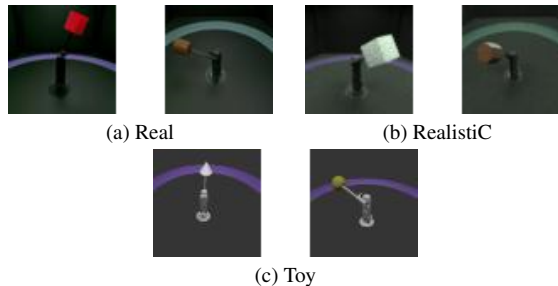


Figure 5. Sample example of different domains in MPI3D.

200 Table 8 outlines the variation factors and their respec-
 201 tive values in the dSprites dataset to provide a comprehen-
 202 sive overview of the dataset. The variation factors include
 203 Scale, Orientation, Position X, Position Y, and Shape Y. It
 204 is worth noting that our study follows a similar setup to pre-
 205 vious works, where Scale represents the size of the shape,
 206 and Position X and Position Y are utilized to determine the
 207 spatial position of the shape within the image.
 208 **MPI3D**: The MPI3D dataset consists of images of 3D ob-
 209 jects in three distinct domains, namely Toy (T), RealisticC
 210 (RC) and ReaL (RL). Figure 5 showcases sample examples
 211 from each domain, highlighting the variations in appearance
 212 and characteristics.

213 We present the variation factors and their respective val-
 214 ues in Table 9 to provide insights into the dataset charac-
 215 teristics. Our study aligns with previous works, adopting a

similar setup where the regression tasks focus on the Hori- 216
 zontal and Vertical Axis. 217

Factor	Values	Task
Horizontal Axis	40 values in $[0, 39]$	Regression
Vertical Axis	40 values in $[0, 39]$	Regression
Object color	6 values	Classification
Object shape	6 values	Classification
Object size	2 values	Classification
Camera height	3 values	Classification
Background Color	3 values	Classification

Table 9. Variations Factors values in MPI3D dataset

Biwi Kinect: The Biwi Kinect dataset is another dataset 218
 considered in our evaluation for domain adaptation in re- 219

gression tasks. It provides data related to head pose estimation, capturing variations in yaw, pitch, and roll angles for both Male (**M**) and Female (**F**) subjects.

Table 10 presents the variation factors and their respective values in the Biwi Kinect dataset. These factors are essential for understanding the dataset’s characteristics and their relevance to regression tasks.

Factor	Values	Task
Yaw	Values $\in [-92.044, 231.352]$	Regression
Pitch	Values $\in [-87.7066, 246.684]$	Regression
Roll angle	Values $\in [754.182, 1297.45]$	Regression

Table 10. Variations Factors values in Biwi Kinect dataset

SmallNorb: The SmallNorb dataset, which has not been previously used for domain adaptation tasks, is included in our evaluation. It consists of samples with different lighting conditions, as shown in Figure 6. We grouped the six lighting conditions into two categories: Dark (**D**) and Bright (**B**).



Figure 6. Sample example of different domains in SmallNorb.

Table 11 presents the variation factors and their respective values in the SmallNorb dataset. The dataset includes variations in lighting conditions, elevations, and azimuths. Specifically, the azimuths ranging from 0° to 340° were employed as the target task in our study.

Factor	Values	Task
Lighting conditions	6 values	Classification
Elevations	9 values in $[30^\circ, 70^\circ]$	Regression
Azimuths	18 values in $[0^\circ, 340^\circ]$	Regression

Table 11. Variations Factors values in SmallNorb dataset

8. Limitations

Real-world scenarios often pose challenges, such as unaligned or missing labels. In this paper, we did not specifically address partial set and open set unsupervised domain adaptation for regression settings. Exploring and developing strategies to handle these scenarios would be a promising avenue for future research.